## JOURNAL OF NANO AND MATERIALS SCIENCE RESEARCH

Volume 3, No.2 (Special Issue, 2025), pp. 36 – 43 Available online at journals.nanotechunn.com/jnmsr



# **ORIGINAL ARTICLE**

# A Comparative Study of the Structural and Optical Properties of Sol-gel Synthesized MgO Nanoparticles for Possible Applications

M. O. Duru<sup>a,\*</sup>, O. K. Echendu<sup>a,b</sup>, F. C. Eze<sup>a</sup>, C. A. Madu<sup>a,b</sup>, J. C. Echewodo<sup>a</sup>, S. J. Motloung<sup>c</sup>, and A. U. Yimamu<sup>c,d</sup>

## KEYWORDS

# Magnesium oxide, Nanoparticle, Sol-gel, Precursor, Optical property

#### ARTICLE HISTORY

Received: July 03, 2025 Revised: September 08, 2025 Accepted: September 17, 2024 Published: November 04, 2025

## ABSTRACT

This study presents the sol-gel synthesis of MgO using Mg(NO<sub>3</sub>)<sub>2</sub>.6H<sub>2</sub>O and MgCl<sub>2</sub>.H<sub>2</sub>O precursors. The as-synthesized MgO from both precursors were annealed at 800°C for 2 hours to improve their quality. The annealed samples were analyzed employing X-ray diffraction (XRD) and ultraviolet-visible (UV-VIS) spectrophotometry to evaluate how precursor type affects the structural and optical properties of MgO nanoparticles. XRD investigation indicated a polycrystalline cubic structure of MgO nanoparticles from both precursors, with preferred orientation in the (210) plane for the chloride-derived sample and in the (200) plane for the nitrate-derived sample. The estimated average crystallite size of MgO from the chloride is approximately twice that from the nitrate, with specific values of ~ 15 nm and ~ 7 nm respectively. UV-VIS diffuse reflectance spectrophotometry revealed that the band gap energies of the MgO from both salts were similar with specific values of 5.69 eV and 5.75 eV for the nitrate-derived sample and the chloride-derived sample, respectively.

# 1 Introduction

Extensive progress has been made in the study of creating and utilizing nanomaterials over an extended period of time [1] – [5]. The exceptional physical properties of nanoparticles make them highly significant for several technological applications. The unique characteristics of nanomaterials, such as enhanced damping [6], mechanical stability [7], improved thermal conductivity [8], and increased strength [9], make them very appropriate for various technological applications.

Magnesium oxide (MgO) exhibits a face-centered cubic (FCC) NaCl-type crystal structure with space group Fm-3m [10]. The unique features of magnesium oxide nanoparticles, such as

chemical inertness, electrical insulation, optical transparency, high temperature stability, high thermal conductivity, high dielectric constant, and biocompatibility, make it an intriguing functional material [10] – [12]. These qualities have made MgO a potential material for numerous scientific and industrial applications such as in photocatalysis, refractory materials, heating apparatuses, optical coatings, sensors, water treatment, antimicrobial activity, adsorbent, and additive in fuel [13] – [18].

MgO nanoparticles have been synthesized by various techniques such as thermal evaporation [19], spray pyrolysis [20], laser vaporization [21], chemical vapour phase transport [22], sol-gel [23], and hydrothermal reaction [22]. Among these techniques, sol-gel has become the most fascinating synthesis technique due to its ability to retain a good

<sup>&</sup>lt;sup>a</sup>Department of Physics, School of Physical Sciences, Federal University of Technology Owerri, P.M.B. 1526, Owerri, Nigeria.

<sup>&</sup>lt;sup>b</sup>Africa Centre of Excellence in Future Energies and Electrochemical Systems (ACE-FUELS), Federal University of Technology, P.M.B. 1526 Owerri, Nigeria.

<sup>&</sup>lt;sup>c</sup>Department of Physics (Qwagwa Campus), University of the Free State, Private Bag, X13, Phuthaditjhaba, 9866, South Africa.

<sup>&</sup>lt;sup>d</sup>Department of Physics, Dire Dawa University, Dire Dawa, Ethiopia

<sup>\*</sup> CORRESPONDING AUTHOR | M. O. Duru, 🖂 miletus.duru@futo.edu.ng

<sup>©</sup> The Authors 2025. Published by JNMSR. This is an open access article under the CC BY-NC-ND license.

stoichiometric ratio, cost effectiveness, small and homogenous particle sizes at relatively low temperature, and ability to maintain chemical uniformity at the molecular level [23] – [27]. Many factors such as annealing temperature, pH, catalyst, precursor solution and environmental conditions affect the properties of materials produced by the sol-gel technique [28].

Balakrishnan et al. [8] investigated the microstructure, optical, and photocatalytic properties of MgO nanoparticles synthesized via the combustion method using magnesium nitrate as a precursor. Mamta et al. [9] also studied the synthesis of nanostructured MgO by sol-gel technique employing magnesium nitrate as precursor and its characterization. Muhammad Umair [29] in the same vein reported on the synthesis and characterization of nanoparticles of MgO using MgCl<sub>2</sub> as a starting material.

In the present work, the influence of two different precursors (magnesium nitrate and magnesium chloride) on the crystallite size, strain  $\epsilon$ , dislocation density  $\delta$ , and the optical properties of sol-gel synthesized MgO nanomaterials has been investigated, as such a comparative study has not, to our knowledge, been previously reported in a single publication. The attained outcomes provided useful information regarding structural and optical properties of MgO, that are highly helpful for optimizing MgO nanomaterials for applications in catalysis, sensing, or optoelectronics. This study provides novel insights that may guide future research on MgO-based nanomaterials.

## 2 Experimental method

#### 2.1 Materials

Magnesium nitrate hexahydrate [Mg (NO<sub>3</sub>)<sub>2</sub>.6H<sub>2</sub>O] (Sigma Aldrich, 98.0%), here referred to as MN and magnesium chloride monohydrate [MgCl<sub>2</sub>.H<sub>2</sub>O], (Sigma Aldrich, 98.6%), Citric acid [C<sub>6</sub>H<sub>8</sub>O<sub>7</sub>] (Sigma Aldrich, 97.2%), and deionized water. Other materials used include an electrical hotplate with a magnetic stirrer, magnetic stirrer rods, beakers and a Ph meter.

# 2.2 Synthesis Technique

Magnesium nitrate hexahydrate (Mg (NO<sub>3</sub>)<sub>2</sub>.6H<sub>2</sub>O) labeled as MN and magnesium chloride monohydrate (MgCl<sub>2</sub>.H<sub>2</sub>O) referred to as MC were used as starting materials to prepare different precursor solutions for the synthesis of MgO. The synthesis starting solutions were prepared by dissolving 0.5 mol of each of the magnesium salts and 1.5 mol of citric acid (C<sub>6</sub>H<sub>8</sub>O<sub>7</sub>) in two 30 ml of deionized water into different beakers to form precursor solutions.

The transparent solutions were stirred continuously for 3 hours at temperature of 80°C, on a magnetic stirrer with heating capability to form a yellow precipitate. Then, the stabilized yellow precipitate was constantly heated and stirred at a temperature of 95 °C.

During the process, the viscosity and colour changed as the precipitate turned to viscous gel. The gel was further calcined to 120 °C for 2 hours and a xerogel material was gained. The resulting xerogel material was ground into fine powders using mortar and pestle and annealed at 800 °C for 2 hours in muffle furnace. The resulting powders from both precursors were further ground into fine powder samples, kept in a sealed container for characterizations. The proposed chemical reactions for the formation of MgO from both MN and MC precursors are presented in Equations 1-8.

Upon adding citric acid to Mg(NO<sub>3</sub>)<sub>2</sub>.6H<sub>2</sub>O, magnesium citrate is produced as follows:

Stirring + heating to 
$$80^{\circ}$$
C
$$Mg(NO_3)_2.6H2O_{(aq)} + C_6H_8O_{7(aq)} \longrightarrow C_6H_6MgO_{7(s)(s)} + 7H_2O_{(1)} + N_{2(g)} + 5/2O_{2(g)}$$
(1)

With further stirring and heating to 95°C, magnesium hydroxide is produced from magnesium citrate as follows:

$$\begin{array}{ccc} C_{6}H_{6}MgO_{7(s)} + 7H_{2}O_{(l)} & \xrightarrow{Calcinations~at~120^{\circ}C} & Mg(OH)_{2(s)} + C_{2}H_{4(g)} \\ & + 4CO_{(g)} + 1/2O_{2(g)} + 7H_{2(g)} + 7H_{2}O_{(l)} & (2) \end{array}$$

On calcinations at  $120^{\circ}$  C, water molecules will be expelled in the form of steam as follows:

$$\begin{array}{c} \text{Calcinations at } 120^{\circ}\text{C} \\ Mg(OH)_2 + 7H_2O_{(I)} & \longrightarrow Mg(OH)_2 + 7H_2O_{(g)}(3) \end{array}$$

On further heating at elevated temperature magnesium hydroxide decomposes to produce magnesium oxide thus:

$$Mg(OH)_2 \xrightarrow{Heating} MgO_{(s)} + H_2O_{(g)}$$
 (4)

For the formation of MgO from magnesium MgCl<sub>2</sub>.H<sub>2</sub>O and citric acid, similar steps are obtained as follows:

With further stirring and heating to 95°C, magnesium hydroxide is produced from magnesium citrate as follows:

$$C_6H_6MgO_{7(aq)} + H_2O_{(l)} \xrightarrow{\text{Heating at 95°C}} Mg(OH)_{2(s)} + C_2H_{4(g)} + 4CO_{(g)} + H_2O_{(l)} + 1/2O_{2(g)}$$
 (6)

On calcinations at 120 °C, water molecules will be expelled as steam as follows:

Calcinations at 
$$Mg(OH)_2(s) + H_2O_{(l)} \xrightarrow{120^{\circ}C} Mg(OH)_{2(s)} + H_2O_{(g)} (7)$$

On further heating at elevated temperature magnesium hydroxide decomposes to produce magnesium oxide thus:

$$Mg(OH)_2$$
 Annealing at  $800^{\circ}C$   $MgO_{(s)} + H_2O_{(g)}$  (8)

## 2.3 Characterizations

The crystal feature of fabricated materials was considered employing X-ray diffraction (XRD) using Bruker AXS diffractometer with Cu-K $\alpha$  wavelength of 0.15418 nm. The optical studies of various samples were performed using UV-Vis spectrophotometry with a Perkin-Elmer Lambda 7505 spectrophotometer, which was used to assess the absorbance, transmittance and diffuse reflectance spectra of various samples.

#### 3 Results and Discussions

#### 3.1 Structural Investigation

Figure 1 shows the X-ray diffraction patterns of MgO nanoparticles synthesized with magnesium nitrate (MN) and magnesium chloride (MC) precursors. Both patterns clearly exhibit the characteristic diffraction peaks of cubic phase MgO at 20 angles of 32.56°, 37.84°, 42.83°, 50.54°, 62.23°, 74.45°, 78.11 which correspond to the (111), (200), (210), (211), (311), (321) and (400) lattice planes, respectively, according to the standard Joint Committee on Powder Diffractions and Standards (JCPDS) reference file No.: 761363. The space group of the structure is Fm-3m. No other impurity phases were discovered within the XRD patterns.

The spectra show a preferential orientation in the (200) plane for the MgO nanoparticle from MN and in the (210) plane for MgO nanoparticles from MC respectively. Comparatively, Figure 1 shows that MgO from MC has stronger and narrower peaks than MgO from MN, indicating better crystallinity.

The values of the lattice parameters calculated from (210) and (200) preferential orientations using Equations 10 and 11 were found to be a=b=c=0.47 nm for MgO material synthesized with MN precursor, and a=b=c=0.48 nm for MgO synthesized with MC precursor, which are close to the lattice parameter value of a=b=c=0.48 nm from the reference JCPDS 761363 file.

The average crystallites sizes calculated using Scherrer's Equation 11 was found to be 7 nm and 15 nm for MgO from MN and MC precursors, respectively. Chloride derived MgO nanoparticles show enhanced crystallinity, and this is experimentally revealed by an upsurge in the intensity of the peak at (210) and the reduction in the full width at half maximum (FWHM) as shown in Figure 1.

The diffraction peak intensity was measured by scanning in the  $2\theta$  range in  $20^{\circ}$  to  $90^{\circ}$  with a step size of  $0.05^{\circ}$ . The interplanar spacing (*d*) and the lattice parameters of the crystals were calculated according to Equations 9 and 10[30] - [31]

$$d_{(hkl)} = \frac{n\lambda}{2\sin\theta} \tag{9}$$

here d stands for interplanar spacing, (hkl) represent Miller indices for each given plane,  $\theta$  is the Bragg's angle,  $\lambda$  is the wavelength of the X-ray and n is the order of diffraction.

$$a = d_{(hkl)}\sqrt{h^2 + k^2 + l^2} \tag{10}$$

where a is the lattice parameter a = b = c for a cubic crystal. The crystallite sizes of nanoparticles were calculated employing Scherrer's Equation 11 [31] – [33]

$$D = \frac{k\lambda}{\beta \cos \theta} \tag{11}$$

where *D* is the crystallite sizes (in nm), k is a constant named shape factor = 0.94,  $\lambda$  is the wavelength of X-ray radiation ( $\lambda$  = 0.15418 nm),  $\beta$  is the full width at half maximum (FWHM)

of the given peak and  $\theta$  is the Bragg angle for the diffraction peak under consideration. Various strains in the crystals trigger shifts within peaks within diffraction lines. This micro-strain prompted distortion in the lattices, hence, the peaks in XRD patterns shift from their normal symmetric shape. This micro strain also triggered by tensile and compressive forces increases the FWHM of diffraction peaks on several occasions. The micro strain, which is the degree of distortion present in MgO crystalline lattice was calculated using Equation 12 [29], [30].

$$Strain(E) = \frac{\beta cos\theta}{4}$$
 (12)

Where  $\theta$  is the  $2\theta$  value of the peak, the dislocation density,  $\delta$  which is the total length of dislocation lines per unit volume in MgO nanoparticle was found using the Equation 13,

$$\delta = \frac{1}{n^2} \tag{13}$$

where D is the crystallite size,  $\theta$  is the Bragg's angle; n is the order of diffraction.

Tables 1 and 2 summaries the variations of structural parameters of MgO synthesized with MN and MC precursors. From Table 1, it is revealed that MgO synthesized with MC precursor has higher values of crystallite size compared with that synthesized with MN.

As Table 2 illustrates, a decrease in lattice defects leads to a reduction in internal strain and dislocation density inside the material. Consequently, the MC grown sample exhibits better crystallization than the MN grown sample. From Table 2, the average micro strain for MgO nanoparticles were 0.0057 and 0.00048 for nitrate and chloride precursors respectively, while the average dislocation densities for MgO are 0.0261 nm<sup>-2</sup> and 0.00048 nm<sup>-2</sup> for MN and MC precursors respectively.

Table 1: Values of 20, inter-planar spacing, FWHM, crystallite size and Miller indices for MgO nanoparticles from nitrate (MN) and chloride (MC) precursors

20	FWHM	Crystallite	d-	hkl	2€	FWHM	Crystallite	d
(Deg)	β (Rad)	size D (nm)	spacing		(Deg)	<b>β</b> (Rad)	size D (nm)	spacing
MN	MN	MN	(nm)		MC	MC	MC	(nm)
			MN					
32.56	0.0286	5.06	0.2750	(111)	32.87	0.0120	12.07	0.2726
37.59	0.0275	5.56	0.2395	(200)	37.85	0.0114	16.08	0.2726
42.51	0.0157	9.91	0.2126	(210)	42.83	0.0132	13.47	0.2111
50.51	0.0339	4.72	0.1807	(211)	50.54	0.0133	11.78	0.1806
61.80	0.0191	8.89	0.1501	(311)	62.23	0.0111	15.10	0.1492
74.15	0.0296	6.14	0.1279	(321)	74.45	0.0100	18.05	0.1274
78.11	0.0246	7.58	0.1223	(400)	78.56	0.0104	17.84	0.1218

Therefore, MgO from MC with a reduced dislocation density can provide a superior lattice and thermal expansion, making it a promising material for high-power radio frequency (RF) devices and ultraviolet (UV) electro-optical applications [34]. Table 1 and 2 show all calculated structural parameters of the two MgO samples.

Table 2: Values of, hkl, micro strain  $\varepsilon$ , and dislocation density  $\delta$ , for nitrate (MN) and chloride (MC) derived samples

(hkl)	Strain, ε	Dislocation	Strain, 8	Dislocation	
	MN	density, $\delta$	MC	density, $\delta$	
		nm <sup>-2</sup> MN		nm <sup>-2</sup> MC	
(111)	0.0069	0.0391	0.0030	0.0065	
(200)	0.0065	0.0323	0.0023	0.0039	
(210)	0.0037	0.0102	0.0031	0.0055	
(211)	0.0077	0.0446	0.0030	0.0072	
(311)	0.0041	0.0127	0.0024	0.0044	
(321)	0.0059	0.0265	0.0020	0.0031	
(400)	0.0048	0.0174	0.0026	0.0032	

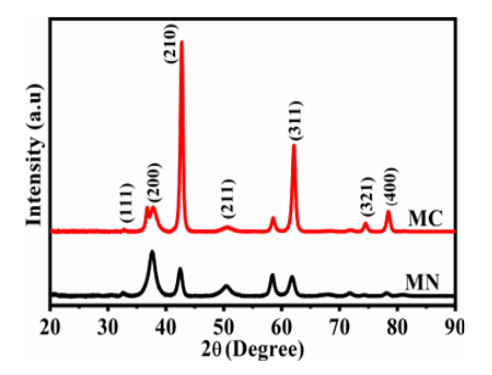


Figure 1: XRD pattern of MN and MC derived MgO nanoparticles

#### 3.2 Optical Analysis

Figure 2(a) presents the graphs of absorbance versus wavelength of MgO nanoparticles synthesized from MN and MC precursors. The graphs show that absorbance decreases from a value of  $\sim 0.25$  to 0.03 as photon wavelength increases in the range of 200-1200 nm (which covers the ultraviolet to near infrared section of the electromagnetic spectrum) for MN sample. Afterward, the absorbance increases from  $\sim 0.03$  to 0.25 in the wavelength range of 1200-2000 nm.

The MC sample generally has higher absorbance values than MN sample with values decreasing from ~0.4 to ~0.1 as photon wavelength decreases in the range of 200 nm – 1800 nm after which it slightly increases to 0.15 as the wavelength increases from 1800 nm to 2000 nm. MC derived MgO can therefore be a much better absorber of electromagnetic radiation than the MN derived sample, suggesting that it may be a preferred candidate for UV-Vis filter applications. There is an observed sharp absorption peak at a wavelength of ~1400 nm in both MgO materials. The origin of this absorption peak cannot be explained at the moment, although it is suspected to be as a result of unknown impurity. Further studies will be required to unravel the true origin.

The band gap energies were evaluated using the Kubelka-Munk function  $F(R\infty)$ , as described in Equations 14 and 15 [35] – [37].

$$F(R_{\infty}) = \frac{\kappa}{s} \tag{14}$$

here  $R_{\infty}$  stands for reflectance, S represent the scattering coefficient, and K signifies absorption coefficient,  $F(R_{\infty})$  is connected to the incident photon energy by the Tauc relation [35] – [36].

$$\{F(R_{\infty})h\nu\}^n = A(h\nu - E_a) \tag{15}$$

where A is a constant,  $h\nu$  represent photon energy,  $E_g$  stands for band gap energy and n transition mode ( $n = \frac{1}{2}$ , n = 2 for allowed direct transition, n = 3 signify direct forbidden transition, and n = 3/2 represent indirect forbidden transition. but the value n = 2 was employed in this work.

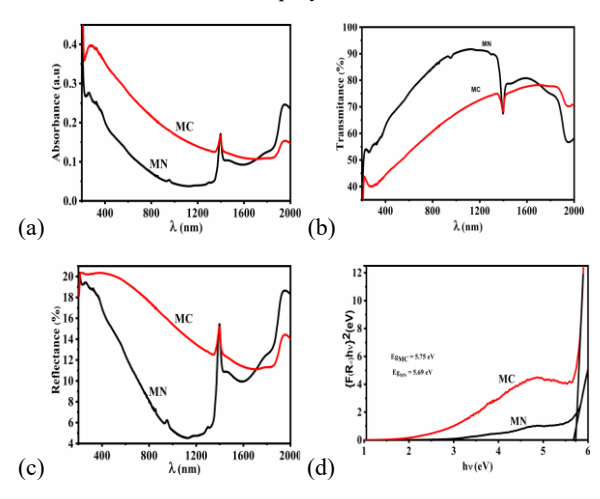


Figure 2: (a) Absorbance (b) Transmittance (c) Reflectance spectra versus wavelength (d)  $\{F(R_\infty)h v\}^2$  against photon energy for MgO nanoparticles synthesized with MN and MC precursors

What makes a substance unique is its complicated dielectric constant. The imaginary part illustrates how a dielectric material absorbs energy from an electric field, while the real part illustrates how much the substance will slow down light. The loss factor, or the ratio of the imaginary to the real parts of the dielectric constant, can be found out by examining the real and imaginary parts of the dielectric constant. Equations 16 and 17 are used to calculate the dielectric constant's real and imaginary portions.

$$\mathcal{E}_r = n^2 - k^2 \tag{16}$$

$$\mathfrak{L}_i = 2nk \tag{17}$$

Where k is the extinction coefficient and n are the refractive index of the material. The absorption coefficient ( $\alpha$ ) associated with the strong absorbance (A) and the thickness (t) of the material is given by Equations 18 and 19 [38] – [44].

$$\alpha = 2.303 \frac{A}{t} \tag{18}$$

$$\alpha = \frac{4\pi k}{\lambda} \tag{19}$$

where  $\lambda$  is the wavelength of the incident electromagnetic radiation. The refractive index was calculated from Equation 20 [39] – [44].

$$n = \frac{1 + R^{1/2}}{1 - R^{1/2}} \tag{20}$$

here R stands for reflectance while the transmittance (T), the reflectance (R) and the absorbance (A) are related using Equation 21.

$$T + R + A = 1 \tag{21}$$

The graphs of transmittance versus wavelength for various MgO nanoparticles employing diverse precursors are shown in Figure 2(b). The results show that the transmittance of MgO nanoparticles from the MN precursor increases from ~43% as the photon wavelength increases from 200 nm with a maximum value of 92% at 1100 nm after which it decreases to about 57% at 2000 nm.

For the MC sample, the transmittance increases more continuously from  $\sim\!\!30\%$  at 200 nm to a maximum value of  $\sim\!\!78\%$  at 1900 nm but for the sudden absorption peak at around 1400 nm and then slightly decreases to 56.69% at 1956 nm. The MgO nanoparticle from the nitrate precursor therefore has overall higher transmittance in the wavelength range of 200 – 2000 nm compared to the MgO nanoparticles from the chloride precursor. The MgO nanoparticles were seen to be significantly transparent in the visible section of wavelength and can be used as an important material with wide applications such as in optoelectronic devices, photocatalytic system and anti-reflection coating as discussed in the literature.

Figure 2(c) illustrates the diagram of reflectance against the wavelength's spectrum for MgO nanoparticles from both precursors. The results show that reflectance of MgO nanoparticle from the nitrate, MN precursor decreases from  $\sim$  18% to  $\sim\!4\%$  as the wavelength increases from  $\sim\!400$  nm to  $\sim$  1000 nm, which covers the visible and near the onset of infrared region of the electromagnetic spectrum. Thereafter, the reflectance increases from  $\sim\!4.5\%$  to 14.5% in the wavelength range of  $\sim\!1000-1300$  nm. MgO nanoparticle from chloride, MC precursor generally has higher reflectance values than the MN sample with the value decreasing from  $\sim\!20-12.5\%$  in the wavelength range from  $\sim\!200$  nm to  $\sim\!1300$  nm.

Using the Tauc relation of Equation 15 and the Kubelka-Munk Equation 14 based on optical absorption spectra, the materials' optical band gap energies,  $E_g$ , were calculated. Figure 2(d) displays the  $(F(R_\infty)hv)^2$  versus  $h\nu$  plots of MgO nanoparticles synthesized from MN and MC precursors annealed at 800 °C. By extending the linear portion of the plot  $(F(R_\infty)hv)^2$  against hv, to the hv axis where  $F(R_\infty)$  equals zero, one may find the optical band gap  $E_g$  value. It was discovered that the two MgO materials' optical band gap values were similar, with particular values of 5.69 eV and 5.75 eV for the MN and MC precursors, respectively.

The degree of crystallinity may influence the difference in band gap energy. The band gap values are consistent with those of Kumar *et al.* [19], who measured the MgO band gap energy at various temperatures ranging from 5.0 eV to 6.2 eV. The bulk value of 7.80 eV found by Kurth *et al.* (7.8 eV) [46] is greater than the band gap values found for both MgO materials from

the precursors in the current work. The technique used and, consequently, the distribution of defects in the material could be the cause of this observed smaller band gap.

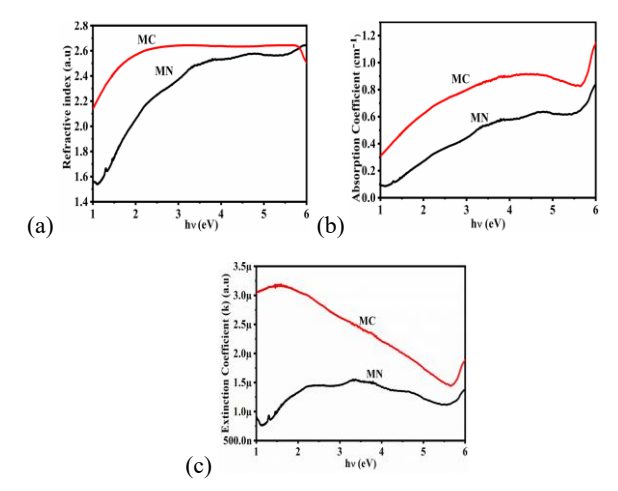


Figure 3: (a) Refractive index, n (b) Absorption coefficient, α (c) Extinction coefficient, k against photon energy for MgO nanoparticles from MN and MC precursors

Figure 3(a) shows the refractive index of MgO nanoparticle from both precursors as a function of photon energy. The refractive index rises as the photon energy increase for MgO nanoparticles from MN and MC precursors. It is also observed that the refractive index of MgO from MN increases from 1.6 to 2.7 in the photon energy range of 1.0 eV to 6.0 eV while the refractive index, *n* of MgO from MC precursor increases from 2.1 to 2.6 within the UV-visible energy region and maintains a constant value of 2.6 from 3.0 eV to 6.0 eV. The higher value of refractive index, of MgO nanoparticles from MC precursor in this photon energy region is important.

Refractive index is a measure of how light propagates through a material. The formula n = c/v, where c is the speed of light in vacuum, states that the higher the refractive index, the slower the speed of light propagation [41]. As a result, light from the MC precursor will travel through MgO more slowly.

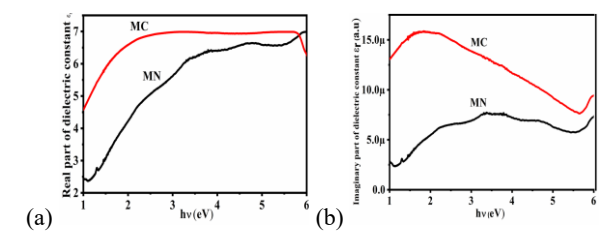


Figure 4: (a) Real dielectric  $\varepsilon_r$  (b) Imaginary dielectric  $\varepsilon_i$  versus photon energy of MgO nanoparticles from MN and MC precursors

The plots of absorption coefficient ( $\alpha$ ) versus photon energy for the MgO nanoparticles made from various precursors are shown in Figure 3(b). When the photon energy of MgO nanoparticles derive from MN and MC precursors increases, the absorption coefficient,  $\alpha$ , also rises. The absorption coefficient of MgO from MN precursor increases from 0.1 cm<sup>-</sup>

<sup>1</sup> to 0.6 cm<sup>-1</sup> in the photon energy range of 1.0 eV to 5.5 eV and then sharply increases from 0.6 cm<sup>-1</sup> to 0.8 cm<sup>-1</sup> within the energy range of 5.5 to 6.0 eV, according to the graphs. In contrast, MgO from MC precursor increases in the photon energy range of 1.0 eV to 5.5 eV from 0.3 cm<sup>-1</sup> to 0.8 cm<sup>-1</sup> and then sharply increases from 0.8 cm<sup>-1</sup> to 1.2 cm<sup>-1</sup> in the range of 5.5 eV to 6.0 eV.

A graph of MgO nanoparticles from MN and MC precursors' extinction coefficient, k, vs photon energy is displayed in Figure 3(c). The observed pattern indicates that the extinction coefficient, k, for MgO synthesized from MN precursor rises as photon energy rises in the range of 1.0 eV to 3.0 eV, stays relatively constant from 3.0 eV to 5.5 eV, and then rises once more.

Conversely, for MgO synthesized from MC precursor, the extinction coefficient decreases as photon energy rises from 1.0 eV to 5.5 eV and then increases as the energy increases 5.5 eV to 6.0 eV. The increase in the extinction coefficient, k of MgO from MN precursor within the 1-3 eV energy range indicates a rise in light loss due to scattering and absorption. Conversely, the decrease in the extinction coefficient of MgO from MC precursor in the energy range of 1.0-5.5 eV, suggests a decrease in the fraction of light lost due to scattering and absorption.

The change in photon energy (hv) for MgO nanoparticles from both precursors is depicted in Figure 4(a) for the real component of the dielectric constant,  $\varepsilon_r$ . The obtained results demonstrate that for MgO nanoparticles from both precursors, the actual dielectric constant increases with a rise in the photon energy. With MgO nanoparticles from MN, the actual dielectric constant rises from approximately 2.4 to 6.6 in the photon energy range of 1.0 eV to 5.0 eV, while it rises from approximately 4.6 to 7.0 in the photon energy range of 1 eV to 3.0 eV and then maintains a constant value of around 7.0 in the region of 3.0 - 6.0 eV.

In the photon energy range of 1.0 eV to 5.70 eV, the real component of the dielectric constant for the MC sample is larger than for the MN sample. Since  $\varepsilon_r$  lowers the speed at which electromagnetic waves propagate through a material, this indicates a greater absorption due to free carriers effects in MgO from MC than in MgO nanoparticles from MN. Figure 4(b) shows the imaginary part of the dielectric constant  $\varepsilon_r$  versus photon energy. The imaginary dielectric constant,  $\varepsilon_r$  trails accurately similar movement with the extinction coefficient (k) as shown in Figure 3(c) for MgO from MN and MC precursors. The minimum value of imaginary dielectric constant  $\varepsilon_r$  of MgO from MN is  $\sim 1.0 \times 10^{-5}$  at 1.0 eV while it is  $1.0 \times 10^{-8}$  for MgO from MC at energy of  $\sim 5.58$  eV

## 4 Conclusion

MgO nanoparticles have been successfully synthesized by citrate sol-gel technique using two Mg precursors. The structural and optical results agreed with earlier work in the literature on MgO nanoparticles. The precursor type

contributed significantly to the structural and optical properties of the synthesized MgO nanoparticles. The observed results suggest that MgO nanoparticles generated from sol-gel technique exhibit remarkable properties suggesting a promising candidate for materials in several scientific and technological applications such as protective layers, photocatalysis, sensors, refractory materials, optical coatings, energy storage devices, etc.

## **Declaration of Competing Interest**

The authors disclose no personal or financial conflicts that might have affected the research.

#### References

- [1] Słońska, A., Kaszewski, J., Wolska-Kornio, E., Witkowski, B., Mijowska, E., Luminescent properties of ZrO2: Tb nanoparticles for applications in neuroscience. Optical Materials(2016) 59: 96-102.
- [2] Xiong, C., Wang, W., Tan, F., Luo, F. Chen, J., Investigation on the efficiency and mechanism of Cd(II) and Pb(II) removal from aqueous solutions using MgO nanoparticles. journal of hazardous materials(2015) 299: 664-674.
- [3] Neppolian, B., Wang, Q., Yamashita, H., Choi, H., Synthesis and Characterization of ZrO2-TiO2 Binary Oxide Semiconductor Nanoparticles: Application and Interparticle Electron Transfer Process. Applied Catalysis A (2007) General 333: 264-271.
- [4] Klubnuan, S., Amornpitoksuk, P., Suwanboon, S., Structural, Optical and Photocatalytic Properties of MgO/ZnO Nanocomposites Prepared by a Hydrothermal Method. materials science in semiconductor processing (2015) 39: 515-520.
- [5] Moustata, M.I., Saleh, I.A., and Abdelhamid, M.R., Synthesis of MgO nanoparticles from Different Organic Precursors, Catalystic Decontamination of Organic Pollutants and Antitumor Activity: J. Materials. Sci Eng 2017, 6:4.
- [6] Tamboli, S.H., Patil, R., Kamat, S., Puri, V., Puri, R., Modification of Optical Properties of MgO thin films by vapour chopping. J Alloys Compd 2009;477:855–9.
- [7] Gray, J.E and Luan, B, *Protective Coatings on Magnesium and its Alloys- a critical review.* Journal of Alloys and Compounds 2002; 336: 88-113.
- [8] Balakarishna, G., Velavan, R., Khalid Mujasam Batoo, Emad H. Raslan. : Microstructure, Optical and Photocatalytic Properties of MgO Nanoparticle. Results in Physics (2020): 16 103013
- [9] Mamta Sharma, Dimple Grandhi and Minakshi Sharina., Synthesis of Nanostructured Magnesium Oxide by Sol-gel Method and its Characterization. IJPSR (2018), Volume 9, issue 4

- [10] Zulkefle, H., Ismail, L.N., Abu Bakar, R., and Mahmood, M.R., Molar Concentration Effect on MgO Thin Films Properties, IEEE Symp. Ind. Electron. Appl. ISIEA (2011) 468. doi:10.1109/ISIEA.2011.6108754.
- [11] Kim, H.W. and Shim, S.H., Growth of MgO Nanowires Assisted by the Annealing Treatment of Au-coated Substrates, Chemical Physics letters (2006) 422-165. doi: 10.1016/j.cplett.2006.02.062.
- [12] Khalil, Khaled D., Ali, H., Bashal, Mohammed Khalafalla, and Ayman A. Zaki., Synthesis, Structural, Dielectric and Optical Properties of Chitosan- MgO Nanocomposite, Journal of Taibah University for Science (2020) 14-975.
- [13] Venkatachalapathy, V.R., and Murugesan, M.H.R, Characterization of MgO Thin Film Prepared by Spray Pyrolysis Technique Using Perfume Atomizer, J. Mater. Sci. Mater. Electron 31 (2020) 17. doi: 10.1007/s10854-020-04046-7.
- [14] Denny, Y.R., Firmansyah, T., Gustiono, V., and Lee, S.S, Effect of Substrate Temperature on the Electronic Properties of MgO Thin Films on Si (100) Grown by Electron Beam Evaporation, Key Engineering Materials841(2020) 243. doi:10.4028/www.scientific.net/KE M.841.243
- [15] Abe, C., Fern'andez., S and Elhouichet, H, Optical Studies of optical properties of ZnO: MgO thin Films Fabricated by Sputtering from Home- made Stable Oversize Targets. Opt. Int. J. Light Electron Opt. 216 (2020) 164934.
- [16] Sharma, J., Sharma, M., and Basu, S, Synthesis of Mesoporous MgO Nanostructures Using Mixed Surfactants Template for Enhanced Adsorption and Antimicrobial Activity. Journal of Environmental Chemical Engi- neering5(2017) 3429.
- [17] Habibah, Z, Ismail, L.N., Bakar, R.A., and Rusop, M., Influence of Heat Treatment on the Properties of MgO: Thin Films as Dielectric Layer, Proc. IEEE Student Conf. Res. Dev. SCORED 16 (2011) 19. doi: 10.1109/SCOReD.2011.6148700
- [18] Shih, W.C., Wang, T.L., Chiang, M.H., and Wu, M.S, Preparation and characterization of highly c-axis textured MgO buffer layer grown on Si(100) substrate by RF magnetron sputtering for use as growth template of ferroelectric thin film, J. Mater. Sci. Mater. Electron 22 (2011) 430. doi: 10.1007/s10854-010-0155-2.
- [19] Kumar, A., and Kumar, J, On the Synthesis and Optical Absorption Studies of Nano-Size Magnesium Oxide Powder. Journal Physics and Chemistry of Solids vol 69, Issue 11, (2008), p. 2764-2772, https://doi.org/10.1016/j.jpcs.2008.06.143
- [20] Mousa, A.O., Nema, N.A., and Trier, H.S., Study of Structural and Optical Properties for MgO Films Prepared by Using Chemical Spray Pyrolysis

- Technique, Materials Science: An Indian Journal14(2016) 426. (2018)
- [21] Jiu, J., Kurumada, K.I., Tanigaki, M., and Yoshikawa, S, Band Gap Energies of Magnesium Oxide Nanomaterials Synthesized by the Sol-Gel Method. Mater. Lett. 58 (2003), p. 44-47.
- [22] Chadwick, A.V., Poplett, I.J.F., Maitland, D.T.S., Smith, M.E., Band Gap Energies of Magnesium Oxide Nanomaterials Synthesized by the Sol- Gel Method. Chem. Mater. 10 (1998), p. 864-870.
- [23] Nomura, K., Taya, S., Okazawa, A., and Kojima, N., Sol-Gel Synthesis and Dilute Magnetism of Nano MgO Powder Doped with Fe. Hyperfine Interact 226(2014) 161. doi:10.1007/s10751-013-0945-z.
- [24] Aitasalo, T., Holsa, J., Jungner, H., Lastusaari, M., and Niittykoski, J., Comparison of Sol-Gel and Solid-State Prepared Eu<sup>2+</sup> Doped Calcium Aluminates. J. Materials Science, vol. 20(2002), pp. 15–20.
- [25] Dlamini, C., Mhlongo, M.R. Koao, L.F., Motaung, T.E., Hlatswayo., Motloung, S.V., The Effects of Varying the Annealing Period on the Structure and Optical Properties of MgAl<sub>2</sub>O<sub>4</sub>:0.1% Mn<sup>2+</sup> Nanophosphors. J. Am, Ceram. Soc. 75, 1151–2916 (1992)
- [26] Motloung, SV., Tsega, M., Dejene FB., Swart HC., Ntwaeaborwa, OM., Koao LF., Effect of Annealing Temperature on Structural and Optical Properties of ZnAl<sub>2</sub>O<sub>4</sub>: 1.5% Pb<sup>2+</sup> Nanocrystals Synthesized Via Sol-Gel Reaction. J. Alloys and Compounds 2016;677:72– 9.
- [27] Bele, A., Mhongo, M.R. Koao, L.F. Motaung, T.E., Malevu., Hlatshwayo, T.T., Mpelane., M. Mlambo, S.V., Effects of Varying Sm³+ Concentration on the Structure, Morphology and Photoluminescence Properties of the BaAl₂O₄/ CaAl₂O/ Ca₄Al₀O₁₃/Ca₃Al₂O₀: X% Sm³+ (0≤x≤1.9) Mixed Phase using Citrate Sol-Gel Method. Hellyon 8(2022)12573.
- [28] Wang, J.A., Novaro, O., Bokhimi, X., Lopez, T., Gomez, R., Navarrete, J., Lianos., M.E. and Salinas, E.L., Characterization of the Thermal Decomposition of Brucite Prepared by Sol-gel Technique for Synthesis of Nanocrystalline MgO. Mater. Lett. 35 (1998), p. 317–323
- [29] Muhammad Umavir Ahmad Khalid., Synthesis and Chatracterization of Nanoparticle of Magnesium oxide (MgO). International journal of science: Basic and Applied Research. ISSN 2307-4531
- [30] Koao, L.F., Dejene, B.F., Hone, F.G. Swart, H.C., Motloung, S.V. Motaung, T.E., Effects of Octadecylammine Molar Concentration on the Structure, Morphology and Optical Properties of ZnO Nanostructure Prepared by Homogenous Precipitation Method. J. Of luminescence 200, 206-215, 2018.

- [31] Maphiri, V.M., Dejene, B.F., Motaung, T.E., Hlathwayo, T.T., Ndwandwe, O.M., Motloung, S.V., Investigative study of Mn<sup>2+</sup> Concentration on the Structure, Morphology and Photoluminescence of Solgel ZnAl<sub>2</sub>O<sub>4</sub>/ZnO/SrAl<sub>2</sub>O<sub>4</sub>/Sr<sub>3</sub>Al<sub>2</sub>O<sub>6</sub> Mixed Phase Nanophosphor J. nanomat, nanotech. 8(2018) 1-13
- [32] Koao, L.F., Djene, F.B., Swart, H.C., Properties of Flower-like ZnO Nanoparticles Synthesized using the Chemical Bath Deposition. Mater.Sci. Semicond. Process. 27(2014)33-40.
- [33] Mhong, M.R., Koao, L.F., Motaung, T.E., Kroon, R.E., Motoung, S.V., Analysis of Nd<sup>3+</sup> Concentration on Structure, Morphology and Photoluminescence of Sol-Gel Sr<sub>3</sub>ZnAl<sub>2</sub>O<sub>7</sub> Nanophosphor. Result in physics 12(2019)1786-1796
- [34] Poulami G, and Mingyuan, H., Effects of Strain on Various Properties and Applications on Onedimensional Nano-/microstructures. J. Mater Sci 2020, htts://doi/10.1007/s10853-020-04500-1
- [35] Kottim G., Reflectance spectroscopy. Springer Verlag .New York 1969
- [36] Lopez. S., Castillo, S., Chavez, J., Diaz, K., Synthesis Characterization Optical electrical and Structural De Peliculas Delgadas de CS2 depositadas por el metodo PECVD.Material 2003; 8:341-9.
- [37] Olivia, F., Avalle, L., Santos, E., Camara, O., Photoelectrochemical Characterization of Nanocrystalline TiO2 films on Titanium Substrates, J. Photochem Photobiol A:Chem 2002; 146: 175-88
- [38] Akinlami, J.O., and Ashamu, A.O., *Optical Properties of GaAs.* J. Of Semi. Vol., 34, No.3V
- [39] Fox M. Optical Properties of Solids., Oxford University Press, 2001:3

- [40] Yu, P Y, Cardona, M., Fundamentals of semiconductors. Berlin: Springer-Verlag, 1996
- [41] Echendu, O.K. and Dharmadasa, M.I., Effects of Thickness and Annealing on Optoelectronic Properties Device Applications. Journal of elect. Mat. Vol.43,No.3, 2014.
- [42] Al-Wardy, R.A., Studying the Effects of Deposition Time on Optical Properties of CdS Thin Films. Journal of Physics: Conf. Series 1032(2018) 012002.
- [43] Onuegbu, S,C., Oluyamo, S.S., Olusola., O.I., Influence of Bath pH value on the Structural and Optical Properties of Electrodeposited MgO Thin Films for Optoelectronic Applications. J. of the Nigeria Society of Physical Sciences.5(2023)931
- [44] Adenyi Yisau Fasasi, Edward Osagie, David Pelemo, Eusebius Obiajunwa, Emmamuel Ajenifuja, John Ajao, Gabriel Osinkolu, Wasiu Oladotun Makinde, Abiodun Eyitayo Adeoye., Effect of Precursor Solvents on the Optical Properties of Copper Oxide Thin Films Deposited Using Spray Pyrolysis for Optical Applications American Journal of Materials Synthesis and Processing 2018,3(2); 12-22, 10.11648/j.ajmsp. 20180302.12
- [45] Oluyamo, Sunday Samuel, Lawrence Olakunle Akiboyewa, Ibiyinka Agboola Fuwape, Olajide Ibukun-Olu Olusola, and Mathew Adefusika Adekoy., Influence of nanocellulose concentration on the tunability of energy bandgap of cadmium telluride thin films. Cellulose 27 (2020)8147.
- [46] Kurth, M., Graat, P.C.J., Mittemeijer., E.J., The Oxidation Kinetic of Magnesium at low Temperatures and low Oxygen partial Pressures Thin Solid Films 500(1) (2006), p. 61-69, DOI: 10.1016/j.tsf.2005.11.044